Measurement of submicrometre diameters of tapered optical fibres using harmonic generation

Ulrich Wiedemann,[1,*] Konstantin Karapetyan[1], Cristian Dan[1], Dimitri Pritzkau[1], Wolfgang Alt[1], Stephan Irsen[2], and Dieter Meschede[1]

[1]Institut für Angewandte Physik, Universität Bonn, Wegelerstr. 8, 53115 Bonn, Germany
[2]Research Center Caesar, Ludwig-Erhard-Allee 2, 53175 Bonn, Germany
**wiedemann@iap.uni-bonn.de*

Abstract: Applications of subwavelength-diameter optical fibres in nonlinear optics require precise knowledge of the submicrometre fibre waist diameter. We demonstrate a new technique for optical measurement of the diameter based on second- and third-harmonic generation with an accuracy of better than 2%. To generate the harmonic light, inter-modal phase matching must be achieved. We find that the phase-matching condition allows us to unambiguously deduce the fibre diameter from the wavelength of the harmonic light. High-resolution scanning electron microscope imaging is used to verify the results.

OCIS codes: (060.2270) Fiber characterization; (190.2620) Harmonic generation and mixing; (190.4160) Multiharmonic generation; (190.4370) Nonlinear optics, fibers

References and links

1. G. Brambilla, F. Xu, P. Horak, Y. Jung, F. Koizumi, N. P. Sessions, E. Koukharenko, X. Feng, G. S. Murugan, J. S. Wilkinson, and D. J. Richardson, "Optical fiber nanowires and microwires: fabrication and applications," Adv. Opt. Photon. **1**(1), 107–161 (2009).
2. M. A. Foster, A. C. Turner, M. Lipson, and A. L. Gaeta, "Nonlinear optics in photonic nanowires," Opt. Express **16**(2), 1300–1320 (2008).
3. L. Tong, R. R. Gattass, J. B. Ashcom, S. He, J. Lou, M. Shen, I. Maxwell, and E. Mazur, "Subwavelength-diameter silica wires for low-loss optical wave guiding," Nature **426**(6968), 816–819 (2003).
4. R. R. Gattass, G. T. Svacha, L. Tong, and E. Mazur, "Supercontinuum generation in submicrometer diameter silica fibers," Opt. Express **14**(20), 9408–9414 (2006).
5. G. Sagué, E. Vetsch, W. Alt, D. Meschede, and A. Rauschenbeutel, "Cold-atom physics using ultrathin optical fibers: light-induced dipole forces and surface interactions," Phys. Rev. Lett. **99**(16), 163602 (2007).
6. F. Warken, E. Vetsch, D. Meschede, M. Sokolowski, and A. Rauschenbeutel, "Ultra-sensitive surface absorption spectroscopy using sub-wavelength diameter optical fibers," Opt. Express **15**(19), 11952–11958 (2007).
7. S. M. Spillane, G. S. Pati, K. Salit, M. Hall, P. Kumar, R. G. Beausoleil, and M. S. Shahriar, "Observation of nonlinear optical interactions of ultralow levels of light in a tapered optical nanofiber embedded in a hot rubidium vapor," Phys. Rev. Lett. **100**(23), 233602 (2008).
8. G. Brambilla, V. Finazzi, and D. J. Richardson, "Ultra-low-loss optical fiber nanotapers," Opt. Express **12**(10), 2258–2263 (2004).
9. S. Leon-Saval, T. Birks, W. Wadsworth, P. St J Russell, and M. Mason, "Supercontinuum generation in submicron fibre waveguides," Opt. Express **12**(13), 2864–2869 (2004).
10. J. Ward, D. O'Shea, B. J. Shortt, M. J. Morrissey, K. Deasy, and S. Nic Chormaic, "Heat-and-pull rig for fiber taper fabrication," Rev. Sci. Instrum. **77**(8), 083105 (2006).
11. F. Warken, A. Rauschenbeutel, and T. Bartholomäus, "Fiber pulling profits from precise positioning," Photon. Spectra **42**(3), 73 (2008).
12. L. Tong, J. Lou, and E. Mazur, "Single-mode guiding properties of subwavelength-diameter silica and silicon wire waveguides," Opt. Express **12**(6), 1025–1035 (2004).
13. G. P. Agrawal, *Nonlinear Fiber Optics* (Academic Press, Orlando, 2001).
14. P. Weidner, and A. Penzkofer, "Spectral broadening of picosecond laser pulses in optical fibres," Opt. Quantum Electron. **25**(1), 1–25 (1993).
15. U. Österberg, and W. Margulis, "Dye laser pumped by Nd:YAG laser pulses frequency doubled in a glass optical fiber," Opt. Lett. **11**(8), 516–518 (1986).
16. U. Österberg, and W. Margulis, "Experimental studies on efficient frequency doubling in glass optical fibers," Opt. Lett. **12**(1), 57–59 (1987).
17. E. M. Dianov, and D. S. Starodubov, "Photoinduced generation of the second harmonic in centrosymmetric media," Quantum Electron. **25**(5), 395–407 (1995).

#124588 - $15.00 USD Received 23 Feb 2010; revised 18 Mar 2010; accepted 19 Mar 2010; published 30 Mar 2010

18. P. G. Kazansky, and P. St. J. Russell, "Thermally poled glass: frozen-in electric field or oriented dipoles?" Opt. Commun. **110**(5-6), 611–614 (1994).
19. P. Dumais, F. Gonthier, S. Lacroix, J. Bures, A. Villeneuve, P. G. J. Wigley, and G. I. Stegeman, "Enhanced self-phase modulation in tapered fibers," Opt. Lett. **18**(23), 1996–1998 (1993).
20. T. A. Birks, W. J. Wadsworth, and P. St. J. Russell, "Supercontinuum generation in tapered fibers," Opt. Lett. **25**(19), 1415–1417 (2000).
21. D. A. Akimov, A. A. Ivanov, A. N. Naumov, O. A. Kolevatov, M. V. Alfimov, T. A. Birks, W. J. Wadsworth, P. St. J. Russell, A. A. Podshivalov, and A. M. Zheltikov, "Generation of a spectrally asymmetric third harmonic with unamplified 30-fs Cr:forsterite laser pulses in a tapered fiber," Appl. Phys. B **76**, 515–519 (2003).
22. V. Grubsky, and A. Savchenko, "Glass micro-fibers for efficient third harmonic generation," Opt. Express **13**(18), 6798–6806 (2005).
23. V. Grubsky, and J. Feinberg, "Phase-matched third-harmonic UV generation using low-order modes in a glass micro-fiber," Opt. Commun. **274**(2), 447–450 (2007).
24. F. Warken, and H. Giessen, "Fast profile measurement of micrometer-sized tapered fibers with better than 50-nm accuracy," Opt. Lett. **29**(15), 1727–1729 (2004).
25. G. Brambilla, and D. N. Payne, "The ultimate strength of glass silica nanowires," Nano Lett. **9**(2), 831–835 (2009).
26. T. A. Birks, J. C. Knight, and T. E. Dimmick, "High-resolution measurement of the fiber diameter variations using whispering gallery modes and no optical alignment," IEEE Photon. Technol. Lett. **12**(2), 182–183 (2000).
27. M. Sumetsky, Y. Dulashko, J. M. Fini, A. Hale, and J. W. Nicholson, "Probing optical microfiber nonuniformities at nanoscale," Opt. Lett. **31**(16), 2393–2395 (2006).
28. A. W. Snyder, and J. D. Love, *Optical Waveguide Theory* (Chapman & Hall, London, 1983), Chap. 12.
29. R. W. Boyd, *Nonlinear Optics*, 2nd ed. (Academic Press, San Diego, 2003), p. 108.
30. M. Baudrier-Raybaut, R. Haïdar, Ph. Kupecek, Ph. Lemasson, and E. Rosencher, "Random quasi-phase-matching in bulk polycrystalline isotropic nonlinear materials," Nature **432**(7015), 374–376 (2004).
31. J. D. Love, and W. M. Henry, "Quantifying Loss Minimisation in Single-Mode Fibre Tapers," Electron. Lett. **22**(17), 912–914 (1986).
32. T. A. Birks, and Y. W. Li, "The Shape of Fiber Tapers," J. Lightwave Technol. **10**(4), 432–438 (1992).
33. B. Rieger, and G. N. A. van Veen, "Method to determine image sharpness and resolution in Scanning Electron Microscopy images," in *EMC 2008 14th Electron Microscopy Congress, Vol. 1: Instrumentation and Methods*, M. Luysberg, K. Tillmann, and T. Weirich, (Springer, Heidelberg, 2008), pp. 613–614.
34. J. S. Villarrubia, A. E. Vladar, J. R. Lowney, and M. T. Postek, "Scanning Electron Microscope Analog of Scatterometry," Proc. SPIE **4689**, 304–312 (2002).
35. E. V. Anoikin, A. N. Guryanov, D. D. Gusovsky, E. M. Dianov, V. M. Mashinsky, S. I. Miroshnichenko, V. B. Neustruev, V. A. Tikhomirov, and Yu. B. Zverev, "UV and gamma radiation damage in silica glass and fibres doped with germanium and cerium," Nucl. Instr. Meth. B **65**(1-4), 392–396 (1992).

1. Introduction

Optical waveguides with submicrometre diameters have attracted much interest in past years [1,2]. This interest was stimulated by the achievement of low losses in optical fibres with diameters down to few hundreds of nanometres [3]. Subsequently, subwavelength-diameter optical fibres (SDOF) have been investigated intensively and a wide range of applications have emerged, e.g. supercontinuum generation [4], evanescent wave spectroscopy of atoms [5] and molecules [6], and nonlinear light-matter interaction in quantum optics [7].

SDOFs can be produced from standard, commercially available optical fibres by the flame-brushing technique [8–11]. The fibre is heated to the viscous condition and, simultaneously, pulled at both ends. Precise computer-controlled pulling technology yields low-loss tapers and a uniform waist. Contrary to a conventional optical fibre, where the light is weakly guided by the core-cladding interface, strong light guidance by the cladding-air interface occurs in the SDOF [12]. This results in tight confinement of propagating mode and thus in high intensity—not only inside the fibre, but also in its evanescent field—and can be compared to a tightly focused beam with an interaction length of up to several centimetres.

Nonlinear processes have been studied in standard optical fibres [13,14], including self-phase modulation (SPM), cross-phase modulation (XPM), stimulated Raman scattering, stimulated Brillouin scattering, and optical solitons. Despite the centrosymmetric properties of silica, second-harmonic generation (SHG) has been observed in optical fibres [15,16] and its origin has been studied [17,18], too.

In comparison to standard optical fibres, the increased intensity in SDOF promises even stronger nonlinear effects. First experiments on spectral broadening by enhanced SPM in SDOF using femtosecond laser pulses had been performed in [19], and were later continued with supercontinuum generation in SDOF [4,20]. Furthermore, third-harmonic generation

#124588 - $15.00 USD Received 23 Feb 2010; revised 18 Mar 2010; accepted 19 Mar 2010; published 30 Mar 2010

(THG) in SDOF was theoretically predicted and experimentally observed [21–23]. In [23], second-harmonic light was also obtained, although its origin remains unclear.

Due to very strong modal dispersion, knowing the waist diameter precisely is critical for quantitatively understanding and controlling light propagation and nonlinear effects in SDOF. Several methods to measure the fibre diameter were proposed. One method is based on illuminating the fibre from the side and then analysing the scattered light. An accuracy of 50 nm for a fibre with a diameter of around 1.32 μm was reported [24]. Scanning electron microscopes (SEM) offer an accuracy of 3% [25], but their use is time consuming and non-destructive measurements are challenging. A method for measuring the uniformity of SDOF with a precision of 2–3% was also proposed [26,27]. However, it gives no information about the absolute diameter, so additional measurements are still required. In this manuscript, we demonstrate a non-destructive method based on SHG and THG to measure the submicrometre fibre diameter with an accuracy better than 2%.

2. Theory

2.1 Light propagation in SDOF

An SDOF can be regarded as a cylindrical glass rod surrounded by air. The light is strongly guided by the cladding-air interface due to the large refractive index step at the SDOF surface. The vector electric field of the propagating mode is given by $\mathbf{E}(r,\varphi,z,t) = \mathbf{E}(r,\varphi)\exp(i\beta z) \times \exp(-i\omega t)$, where $\beta = \omega/v_{ph} = \omega\, n_{eff}/c$. Here, n_{eff} is the effective refractive index, r, φ and z the cylindrical coordinates, $\mathbf{E}(r,\varphi)$ the transverse electric field distribution, t the time, ω the angular frequency of light, v_{ph} the phase velocity, and c the speed of light in vacuum. The full description of light propagation in cylindrical structures can be found in [28].

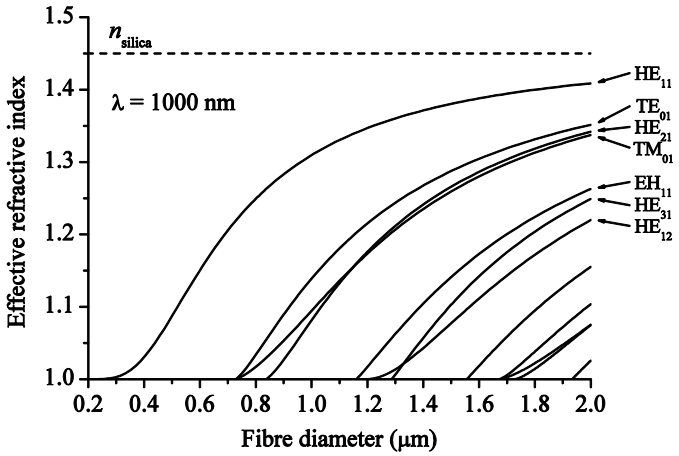

Fig. 1. The effective refractive index of the fundamental mode (leftmost) and the higher modes depending on the fibre diameter. The modes were calculated for $n_{silica} = 1.450$ ($\lambda = 1000$ nm).

To determine the effective refractive index of a cylindrical waveguide, we numerically solve the eigenvalue equation for the step-profile fibre [12,28] taking into account material dispersion and the strong guidance in the subwavelength-diameter fibre. The solutions are the hybrid modes (HE and EH) and transverse modes (TE and TM), for which the effective refractive index n_{eff} is shown in Fig. 1. With decreasing SDOF diameter, a greater percentage of light propagates in the evanescent field in air, and the effective refractive index becomes lower.

2.2 Modal phase matching for harmonic generation

For efficient harmonic generation, phase matching between the fundamental and harmonic light has to be achieved, which means that the phase velocities $v_{ph} = c/n_{eff}$ of fundamental and

#124588 - $15.00 USD Received 23 Feb 2010; revised 18 Mar 2010; accepted 19 Mar 2010; published 30 Mar 2010

harmonic waves have to be equal. This results in the phase matching condition $n_{\text{eff,fundamental}} = n_{\text{eff,harmonic}}$.

Figure 2a shows the effective refractive index for the fundamental and the second-harmonic light. To avoid confusion due to similar values of fibre diameters and wavelengths, we denote the fibre diameter in micrometres and the wavelength in nanometres throughout the paper. The three intersections at different fibre diameters are the phase matching points. If the wavelength is changed, the n_{eff} curves shift, and thus phase matching occurs at a different fibre diameter, see Fig. 2b. This means that for each mode there is a one to one relation between the fibre diameter and the phase-matching wavelength (Fig. 2c).

The phase-matching curves for THG can be obtained in a similar way.

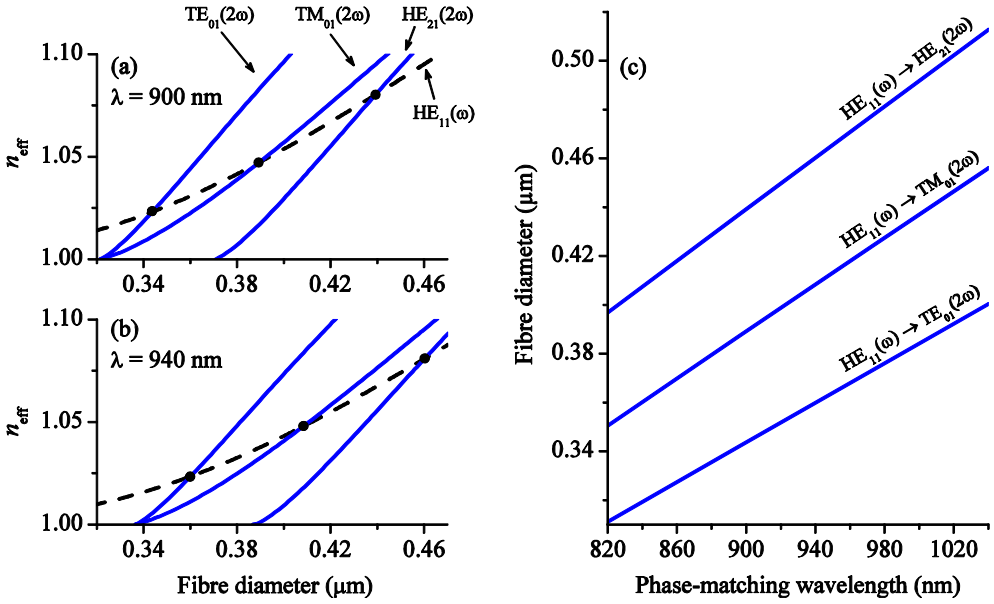

Fig. 2. (a, b) Effective refractive index of the fundamental wave (dashed line) and the second harmonic wave (continuous lines). For each wavelength the phase-matching condition is fulfilled at the three intersections. (c) Dependence of the fibre diameter on the phase-matching wavelength for the three modes.

2.3 Influence of the varying fibre diameter on the harmonic spectral response

In Fig. 3a we have sketched the diameter profile of an ideal SDOF with a finite in length cylindrical section with constant diameter and taper sections with increasing diameters at each end. The frequency of occurrence of the diameters is illustrated in the histogram in Fig. 3b.

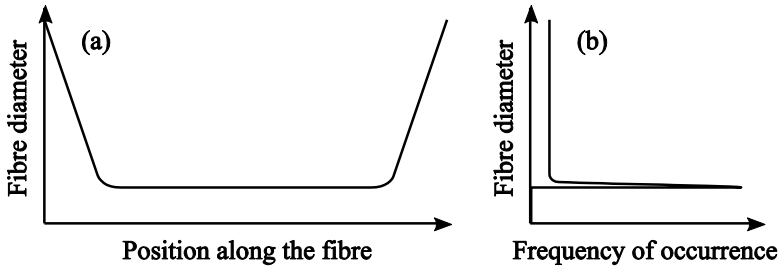

Fig. 3. (a) Sketch of the diameter profile of an SDOF. (b) Frequency of occurrence of the fibre diameters.

Figure 4a shows the diameter profile of one of our samples measured with an SEM. The fibre waist typically exhibits a short thinner section on one or both sides, followed by the taper

#124588 - $15.00 USD Received 23 Feb 2010; revised 18 Mar 2010; accepted 19 Mar 2010; published 30 Mar 2010

region with increasing thickness. For each fibre diameter the phase matching occurs at a certain wavelength. The large variation of the diameter in the tapers will therefore produce a weak broadband harmonic generation response, while the relatively uniform and long waist will cause a narrow peak.

To connect the diameter occurrence in Fig. 4c with the expected harmonic spectral response, i.e. the conversion efficiency vs. the wavelength, one has to know the coherence length l_{coh} (the length over which the phase matching is maintained). For a perfectly uniform waist shape ($l_{coh} \gg l_{waist}$), the conversion efficiency depends quadratically on the waist length, $\eta \sim l_{waist}^2$, due to coherent addition of the field amplitudes [29]. In the realistic case of a non-uniform waist ($l_{coh} \ll l_{waist}$) the dependence will be approximately linear, $\eta \sim l_{waist}$, due to intensity build-up [30].

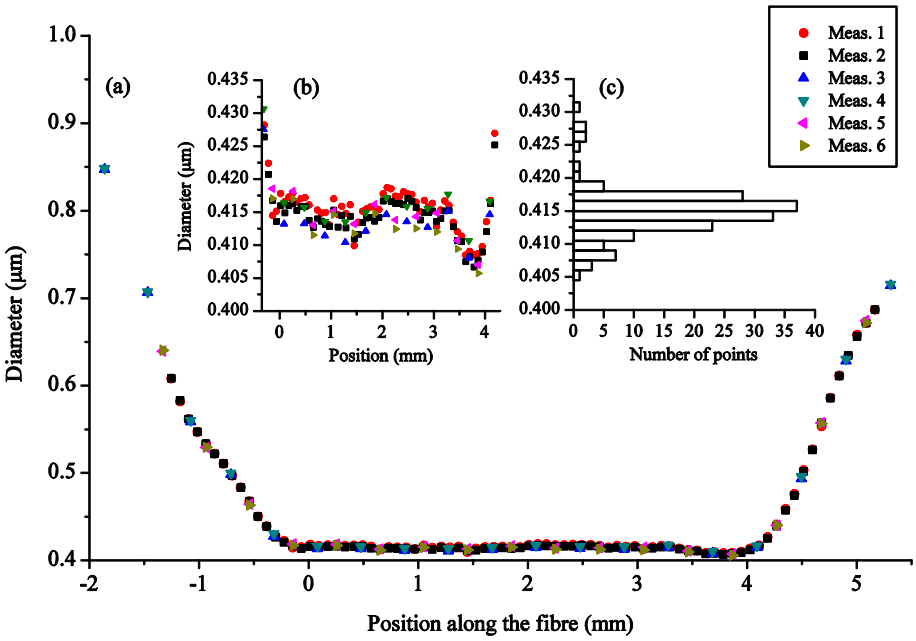

Fig. 4. (a) Diameter profile of an SDOF (sample A) obtained by SEM measurements of different beam energies and scan speeds, designated Meas. 1 to Meas. 6. The position of zero along the fibre is arbitrary. (b) Vertically enlarged picture of the waist. A short thinner region at the right end of the waist can be seen. All the individual points are measured with an accuracy of $<7 \times 10^{-3}$ μm. (c) Diameter histogram.

3. Implementation of the method and experimental results

3.1 Samples

The SDOF samples were pulled from the Fibercore SM800-5.6-125 fibre which has a germanium-doped core (d_{core} = 4 μm) and a pure silica cladding ($d_{cladding}$ = 125 μm). After pulling, a sample consists of an unprocessed fibre section, a down-taper, a subwavelength-diameter waist, an up-taper (which is symmetric to the down-taper), and a second unprocessed section. Each taper consists of three sequential conical sections with slopes of 3 mrad, 2 mrad, and 3 mrad, respectively, and typically has a total length of 3.5 cm. We use the 2 mrad shallow slope section to achieve an adiabatic transition from the core-guided into the cladding-guided mode [31,32]. The fibre waist has a length of 4 mm. The results in this paper are obtained from samples with diameters ranging from 0.32 to 0.51 μm. The samples are labeled with capital letters A–G.

#124588 - $15.00 USD Received 23 Feb 2010; revised 18 Mar 2010; accepted 19 Mar 2010; published 30 Mar 2010

3.2 Setup

Our experimental setup is shown in Fig. 5. To measure SHG and THG at different wavelengths we use a tunable Spectra-Physics Tsunami Ti:Sa laser (840…1020 nm), which can operate in both continuous-wave (CW) and pulsed (1 ps pulse duration, 80 MHz repetition rate) mode. The input fibre end is fixed to a positioning stage and the beam is coupled in using a microscope objective. The typical average power in the sample is 120 mW (1.5 nJ pulse energy). The beam emitted from the fibre is collected by a lens. A dichroic mirror reflects infrared (IR) and transmits the second harmonic. The IR power is monitored by a thermal power meter. The light passing the dichroic mirror (~100 nW) is filtered from residual IR light and the second-harmonic signal is measured by a spectrometer (Avantes AvaSpec 3648–UA-25-AF). Despite higher efficiency of THG in comparison with SHG in silica, we do not observe a significant amount of THG light at the end of the fibre due to the high UV-absorption in the Ge-doped core of our samples. Therefore we measure the third-harmonic signal by positioning an ultraviolet-pass filter and the spectrometer directly above the fibre waist. (Similar to [23], by splicing a pure silica 50 µm core fibre to our fibre sample at the up-taper, we were also able to collect the third-harmonic ultraviolet (UV) light at the end of the fibre.)

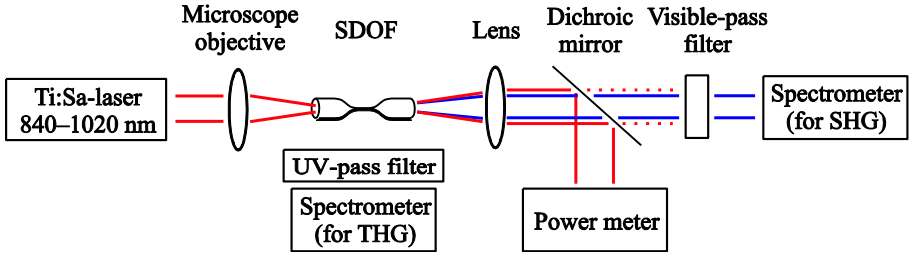

Fig. 5. Experimental setup for SHG and THG measurement.

3.3 Measurement procedure

The pulsed laser and the strong light confinement provide high peak intensity in the waist. This high peak intensity leads to SPM-dominated nonlinear broadening of the IR light. The 1 ps pulse with an initial spectral width of ~1 nm is broadened by 20…30 nm. The IR transmission of the tapered part of the fibre exceeds 95%.

For each broadened spectrum, the resulting second-harmonic light is measured using the spectrometer, see Fig. 6a. To determine the second-harmonic spectral response of the fibre, we scan the whole tuning range of our laser in between 10 and 20 steps and build the envelope of all individual spectra, see Fig. 6b. The same procedure is repeated for THG.

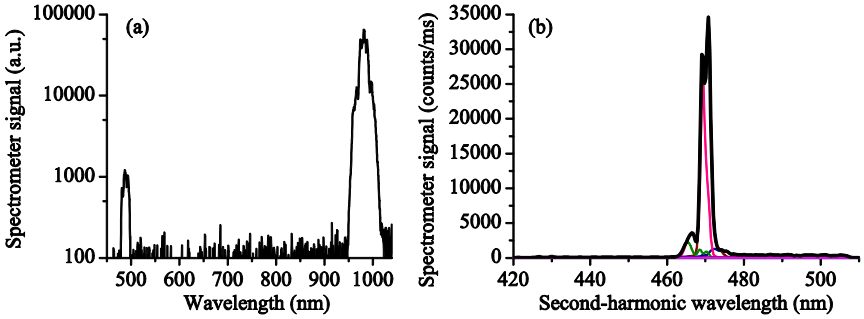

Fig. 6. (a) SHG at a fixed laser wavelength. The spectrally broadened IR light is converted to the second harmonic. Due to different coupling efficiencies of the IR and the second-harmonic light to the spectrometer, the peak heights are not up to scale. (b) Full second-harmonic spectral response of sample A: envelope (thick line) of individual SHG spectra taken at different laser wavelengths (thin lines).

#124588 - $15.00 USD Received 23 Feb 2010; revised 18 Mar 2010; accepted 19 Mar 2010; published 30 Mar 2010

3.4 Analysis

As explained in section 2, the wavelength of the generated second-harmonic light is directly connected to the fibre diameter via the phase-matching condition. Thus, the second-harmonic spectral response shown in Fig. 6b can be analysed with respect to the fibre diameter.

We attribute the second-harmonic tail at long wavelengths to phase matching occurring within the taper. The main peak, originating from the fibre waist, is at λ_{SHG} = 470 nm ($\lambda_{fundamental}$ = 940 nm) and corresponds to phase matching of $HE_{11}(\omega)$ to $TM_{01}(2\omega)$ at a fibre diameter of d = 0.408 µm. The leftmost minor peak corresponds to a short segment (cf. position 3.5 to 4 mm in Fig. 4) being thinner than the rest of the waist. Since there are no regions of smaller diameter in the fibre, there is no possibility of phase matching at shorter wavelengths. This explains the distinct cut-off on the left side of the spectrum.

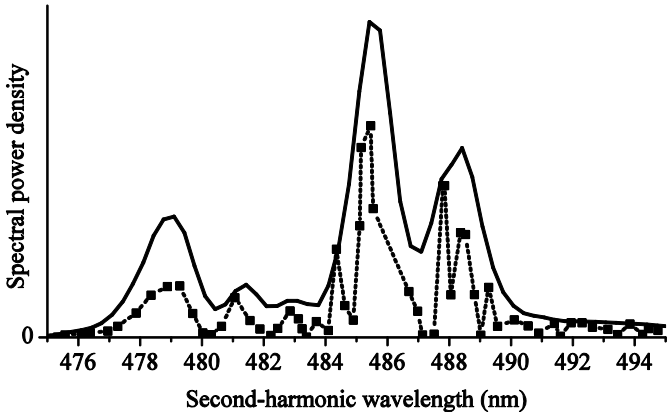

Fig. 7. Second-harmonic spectral response of sample B measured with CW light (dotted line; the solid squares represent the measured points) in comparison to the measurement with pulsed light (continuous line). The heights of the two signals are not up to scale.

The high peak intensity of the picosecond laser pulse could influence the phase-matching condition due to SPM or XPM effects [23]. Thus, we have cross-checked the second-harmonic spectral response of the fibre with a CW measurement using the same average power. Since the intensity of the CW light is much lower than the peak intensity of the pulsed light, the SHG in CW mode is much weaker than in the pulsed mode. Therefore we detect the second-harmonic signal with a photomultiplier tube (PMT). To obtain the spectral response, the laser wavelength is tuned in steps of about 0.4 nm and measured with an optical spectrum analyser (OSA, Ando AQ-6315A). Figure 7 shows the results for the CW and the pulsed measurements. One can see that the shapes in both spectra coincide well, which means that for our intensities nonlinear effects like SPM or XPM seem to have no measurable influence on the phase-matching condition. The double peak structure of the spectrum at 485.5 nm (d = 0.4766 µm) and 488.0 nm (d = 0.4792 µm) could be explained by this particular sample having two dominating waist diameters. The conversion efficiency of SHG with 120 mW of CW light is typically on the order of 10^{-8}.

Figure 8 illustrates how to derive the waist diameter from the peak position of SHG and THG. The full second- and third-harmonic response of sample C is shown in Fig. 8a and the phase-matching condition for SHG and THG is shown in Fig. 8b. The fibre waist diameter is determined from the wavelengths of the four peaks listed in Table 1.

#124588 - $15.00 USD Received 23 Feb 2010; revised 18 Mar 2010; accepted 19 Mar 2010; published 30 Mar 2010

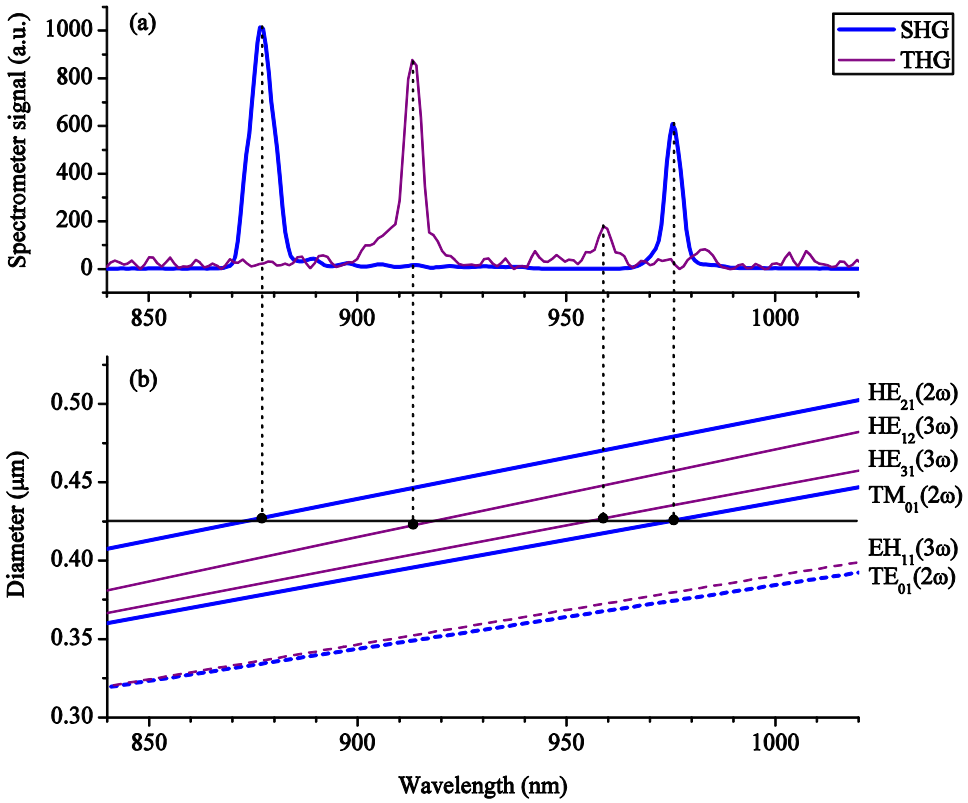

Fig. 8. (a) The spectral response of sample C for SHG (thick line) and THG (thin line) plotted vs. the fundamental wavelength. The spectrometer signal of the THG measurement is scaled up for visibility. The four peaks correspond to phase matching to the following modes (from left to right): $HE_{21}(2\omega)$, $HE_{12}(3\omega)$, $HE_{31}(3\omega)$, $TM_{01}(2\omega)$. (b) Wavelength-dependent phase matching diameter. Thick lines: SHG, thin lines: THG, dashed lines: modes not observed. The horizontal line indicates the diameter of the investigated sample determined by this method.

Table 1. Phase-matching wavelengths and corresponding waist diameters of sample C.

Wavelength (nm)	Phase-matching mode	Diameter (µm)	Diameter error (µm)
877.0	$HE_{21}(2\omega)$	0.427	$\pm 0.8 \times 10^{-3}$
913.5	$HE_{12}(3\omega)$	0.423	$\pm 1.3 \times 10^{-3}$
958.5	$HE_{31}(3\omega)$	0.427	$\pm 1.1 \times 10^{-3}$
976.0	$TM_{01}(2\omega)$	0.426	$\pm 0.7 \times 10^{-3}$

The average fibre waist diameter is 0.4257 µm. The diameter errors in Table 1 are obtained from the spectrometer resolution of ± 0.7 nm and the calibration error of ± 0.3 nm using the phase-matching functions shown in Fig. 8b. Since these individual diameter errors are smaller than the variation of the diameter value, we assume some unknown underlying systematic error. We therefore estimate the diameter error as half of the maximum difference between the diameter values. From Table 1 we receive for sample C the error of $\pm 2.0 \times 10^{-3}$ µm. This value is the largest among all samples A–F. We take a conservative approach and use this value for all our samples.

We have not observed the two modes $TE_{01}(2\omega)$ and $EH_{11}(3\omega)$ in any of our samples falling in the range between 0.32 and 0.4 µm. This could be due to the poor overlap of the fundamental $HE_{11}(\omega)$ to the $TE_{01}(2\omega)$ and $EH_{11}(3\omega)$, due to poor guidance of the $TE_{01}(2\omega)$ and $EH_{11}(3\omega)$ in the fibre waist, or due to coupling losses of these modes in the up-taper.

Note that we observe the mode $HE_{31}(3\omega)$, even though it was predicted that there should be no efficient energy transfer from $HE_{11}(\omega)$ to $HE_{31}(3\omega)$ [22].

#124588 - $15.00 USD Received 23 Feb 2010; revised 18 Mar 2010; accepted 19 Mar 2010; published 30 Mar 2010

3.5 Verification

To verify our method, we check the samples using a Zeiss SUPRA 55 field emission scanning electron microscope (SEM). Before inserting the samples into the SEM, they are attached to a gold-coated silicon wafer and additionally coated by sputtering a 2 nm thick layer of gold using a Bal-Tec MED 020 machine. The coating minimizes distortion of the electric field in the SEM due to electrostatic charging of the non-conductive silica. We use electron acceleration voltages of 15 and 20 kV and calibrate the obtained SEM images with a calibration target (Plano S1995A). To find the edge of the fibre, we use the highest contrast model [33]. More precise models [34] can be used, but they require the exact knowledge of the electron-sample interaction, which depends on the material, geometry and dimensions of the samples.

While the application of SEM is straightforward for relative diameter measurements (imaging the fibre), it is challenging to perform absolute measurements of the submicrometre diameter with an accuracy below 2%. For a fibre of 0.4 μm diameter, this corresponds to an error of $<8 \times 10^{-3}$ μm. As shown in section 3.4, the resolution of our optical method is limited only by the resolution and accuracy of the wavelength measurement and is 0.5×10^{-3} μm when using the OSA instead of the spectrometer.

The comparison of the fibre diameter obtained by harmonic generation and SEM measurements is shown in Table 2 and Fig. 9. The procedure to derive the diameter value and the error for our optical method was described in section 3.4. To get the diameter value of the SEM measurement, we identify the highest peak of the diameter histogram (as shown in Fig. 4c for sample A).

Further on, we calculate the error of the SEM measurement. Each SEM image shows a 1 μm long section of the fibre (see Fig. 10a). The fibre diameter is determined by measuring the distance between the fibre edges on the image. Various contributions to the total diameter error are listed in Table 3. The overall sample diameter error of $\pm 7 \times 10^{-3}$ μm is denoted by the horizontal error bars in Fig. 9. The variation of these various errors along the waist is negligible, therefore we use the same error bar for all measurement positions along the waist.

Table 2. Fibre waist diameters obtained by optical method and SEM

Sample	Fibre diameter (μm)	
	Optical method (± 0.002 μm)	SEM (± 0.007 μm)
A	0.407	0.414
B	0.477	0.485
C	0.426	0.428
D	0.377	0.389
E	0.403	0.419
F	0.503	0.511

#124588 - $15.00 USD Received 23 Feb 2010; revised 18 Mar 2010; accepted 19 Mar 2010; published 30 Mar 2010

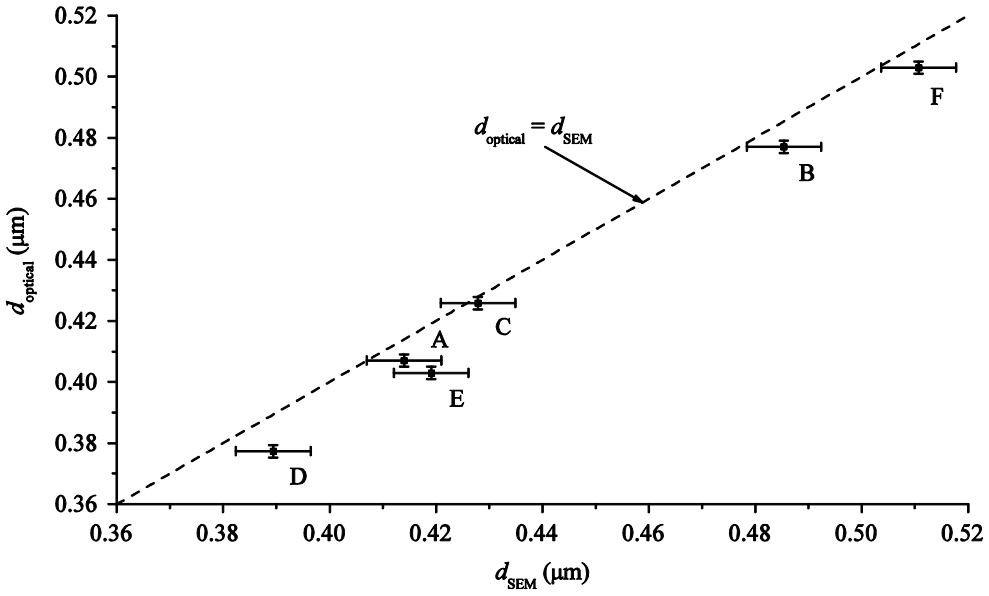

Fig. 9. The fibre diameter measured by harmonic generation ($d_{optical}$) vs. the diameter as measured by SEM (d_{SEM}) for samples A to F.

Table 3. SEM error contributions

Source	Value (μm)	Comment
Finding fibre edge on the image	$\pm 5 \times 10^{-3}$	Systematic uncertainty of our image analysis method
SEM calibration for each beam energy, beam current, scan speed	$\pm 4 \times 10^{-3}$	Error of the calibration target (Plano S1995A), error of processing the target images
Diameter error due to gold coating thickness variation	$\pm 2 \times 10^{-3}$	According to Bal-Tec, manufacturer of our sputtering machine MED 020
Total:	$\pm 7 \times 10^{-3}$	

It is worthwhile to mention that the double peak seen on the spectral curve in Fig. 6b corresponds to the two main diameters seen in the SEM data (Fig. 4b): slightly thinner waist from 0.5 to 2 mm and a thicker part between 2 and 3 mm. The number of SEM images taken is not large enough to allow us to resolve the two peaks in the histogram (Fig. 4c).

3.6 Fibre damage

During our measurements, we have observed in some samples (not included in Fig. 9) a change in harmonic generation properties over time. After exposing the fibres to pulsed light for a longer time (hours), the SHG and THG spectra shifted several nanometres towards longer wavelengths. The SEM investigation of these samples showed that some of them suffered physical modification of the surface: a series of "bumps" are clearly visible on the tapered fibre, see Fig. 10.

#124588 - $15.00 USD Received 23 Feb 2010; revised 18 Mar 2010; accepted 19 Mar 2010; published 30 Mar 2010

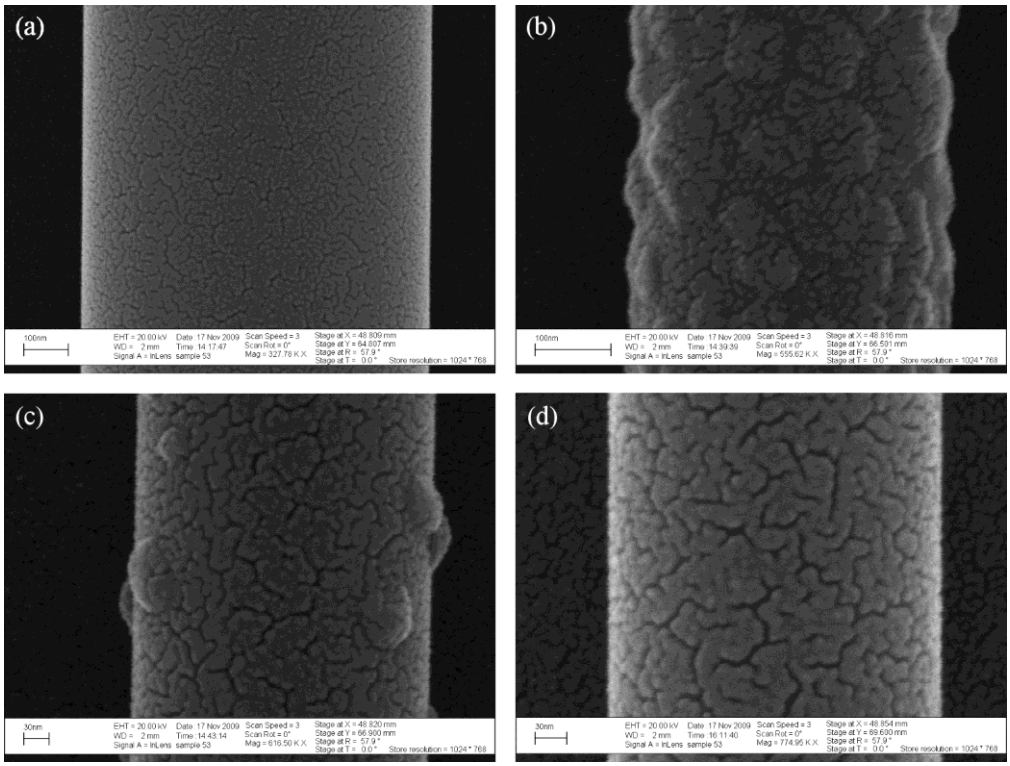

Fig. 10. SEM images of the damaged sample G. No phase matching and therefore no harmonic light could be achieved within our laser wavelength range for (a) a very thick section of the taper (d = 0.790 µm) and (d) for the waist (d = 0.319 µm). Images (b) and (c) show the taper sections where harmonic light was generated (d = 0.430 µm and d = 0.355 µm, respectively). The fissures on all images are due to the gold coating.

While the origin of these bumps is not clear, the result obtained with one particular sample allows us to suggest a cause. This sample G has a ~0.32 µm diameter waist (measured with SEM), which is too thin to produce harmonic generation with the wavelength range of our laser (840…1020 nm). However, this wavelength range provides for phase matching to the second and third harmonic in the diameter range of 0.36…0.5 µm (see Fig. 8b). The taper of sample G covers this whole range. In our setup, we have observed a low second- and third-harmonic signal at all wavelengths of our laser. The SEM images reveal the bumps on the taper just in the diameter range where the harmonics could be generated (Fig. 10b and c). At the same time, no bumps are seen on the thicker section of the taper (Fig. 10a) and on the waist (Fig. 10d), for which phase matching is not achievable. We can thus conclude that the appearance of bumps is related to the generation of harmonic light. In our case, the third harmonic falls into the UV range, which can indeed damage optical fibres [35]. The fibre used in this experiment (Fibercore SM800) is not specified for UV operation.

Therefore, strong harmonic generation can induce irreversible changes in the fibre, including a change of the phase-matching wavelength, which could be problematic for an accurate measurement of the fibre diameter. This can be avoided by using CW light to measure the harmonic spectral response. No peak shift has been observed in our samples while using CW for even longer times.

4. Conclusion

We have presented a method to optically measure the diameter of an SDOF with a resolution of 0.5×10^{-3} µm (limited by the spectrometer or—as in our measurement with CW light—the laser linewidth) and an accuracy of <2% (limited by the SEM used for verification). To

#124588 - $15.00 USD Received 23 Feb 2010; revised 18 Mar 2010; accepted 19 Mar 2010; published 30 Mar 2010

achieve harmonic generation at the phase-matching wavelength, a tunable laser can be used in both pulsed and CW modes. The accessible fibre diameter range is determined by the laser tuning range. Taking into account the transparency window of silica as the limit for light propagation in fibres, one can theoretically measure fibres with diameters down to 0.19 μm with a fundamental wavelength of 500 nm, and fibres with diameters up to 1 μm using fundamental wavelengths up to 2000 nm. Another option to extend the range of accessible diameters is to achieve harmonic generation to another set of higher modes, for which phase matching occurs at different fibre diameters. The straightforward experimental setup and fast measurement procedure makes this technique easily applicable.

Acknowledgments

Financial support by the Deutsche Forschungsgemeinschaft DFG (Research Unit 557) and the European Commission (STREP "CHIMONO") is gratefully acknowledged. We would also like to thank Angelika Sehrbrock for help with electron microscopy measurements.

#124588 - $15.00 USD Received 23 Feb 2010; revised 18 Mar 2010; accepted 19 Mar 2010; published 30 Mar 2010